

Measurement of the Inclusive Jet Cross Section using the k_T algorithm in $p\bar{p}$ Collisions at $\sqrt{s} = 1.96$ TeV

- A. Abulencia,²³ D. Acosta,¹⁷ J. Adelman,¹³ T. Affolder,¹⁰ T. Akimoto,⁵⁴ M.G. Albrow,¹⁶ D. Ambrose,¹⁶
 S. Amerio,⁴² D. Amidei,³³ A. Anastassov,⁵¹ K. Anikeev,¹⁶ A. Annovi,⁴⁵ J. Antos,¹ M. Aoki,⁵⁴ G. Apollinari,¹⁶
 J.-F. Arguin,³² T. Arisawa,⁵⁶ A. Artikov,¹⁴ W. Ashmanskas,¹⁶ A. Attal,⁸ F. Azfar,⁴¹ P. Azzi-Bacchetta,⁴²
 P. Azzurri,⁴⁵ N. Bacchetta,⁴² H. Bachacou,²⁸ W. Badgett,¹⁶ A. Barbaro-Galtieri,²⁸ V.E. Barnes,⁴⁷ B.A. Barnett,²⁴
 S. Baroiant,⁷ V. Bartsch,³⁰ G. Bauer,³¹ F. Bedeschi,⁴⁵ S. Behari,²⁴ S. Belforte,⁵³ G. Bellettini,⁴⁵ J. Bellinger,⁵⁸
 A. Belloni,³¹ E. Ben Haim,⁴³ D. Benjamin,¹⁵ A. Beretvas,¹⁶ J. Beringer,²⁸ T. Berry,²⁹ A. Bhatti,⁴⁹ M. Binkley,¹⁶
 D. Bisello,⁴² M. Bishai,¹⁶ R. E. Blair,² C. Blocker,⁶ K. Bloom,³³ B. Blumenfeld,²⁴ A. Bocci,⁴⁹ A. Bodek,⁴⁸
 V. Boisvert,⁴⁸ G. Bolla,⁴⁷ A. Bolshov,³¹ D. Bortoletto,⁴⁷ J. Boudreau,⁴⁶ S. Bourov,¹⁶ A. Boveia,¹⁰ B. Brau,¹⁰
 C. Bromberg,³⁴ E. Brubaker,¹³ J. Budagov,¹⁴ H.S. Budd,⁴⁸ S. Budd,²³ K. Burkett,¹⁶ G. Busetto,⁴² P. Bussey,²⁰
 K. L. Byrum,² S. Cabrera,¹⁵ M. Campanelli,¹⁹ M. Campbell,³³ F. Canelli,⁸ A. Canepa,⁴⁷ D. Carlsmith,⁵⁸
 R. Carosi,⁴⁵ S. Carron,¹⁵ M. Casarsa,⁵³ A. Castro,⁵ P. Catastini,⁴⁵ D. Cauz,⁵³ M. Cavalli-Sforza,³ A. Cerri,²⁸
 L. Cerrito,⁴¹ S.H. Chang,²⁷ J. Chapman,³³ Y.C. Chen,¹ M. Chertok,⁷ G. Chiarelli,⁴⁵ G. Chlachidze,¹⁴
 F. Chlebana,¹⁶ I. Cho,²⁷ K. Cho,²⁷ D. Chokheli,¹⁴ J.P. Chou,²¹ P.H. Chu,²³ S.H. Chuang,⁵⁸ K. Chung,¹²
 W.H. Chung,⁵⁸ Y.S. Chung,⁴⁸ M. Ciljak,⁴⁵ C.I. Ciobanu,²³ M.A. Ciocci,⁴⁵ A. Clark,¹⁹ D. Clark,⁶ M. Coca,¹⁵
 A. Connolly,²⁸ M.E. Convery,⁴⁹ J. Conway,⁷ B. Cooper,³⁰ K. Copic,³³ M. Cordelli,¹⁸ G. Cortiana,⁴² A. Cruz,¹⁷
 J. Cuevas,¹¹ R. Culbertson,¹⁶ D. Cyr,⁵⁸ S. DaRonco,⁴² S. D'Auria,²⁰ M. D'Onofrio,¹⁹ D. Dagenhart,⁶
 P. de Barbaro,⁴⁸ S. De Cecco,⁵⁰ A. Deisher,²⁸ G. De Lentdecker,⁴⁸ M. Dell'Orso,⁴⁵ S. Demers,⁴⁸ L. Demortier,⁴⁹
 J. Deng,¹⁵ M. Deninno,⁵ D. De Pedis,⁵⁰ P.F. Derwent,¹⁶ C. Dionisi,⁵⁰ J.R. Dittmann,⁴ P. DiTuro,⁵¹ C. Dörr,²⁵
 A. Dominguez,²⁸ S. Donati,⁴⁵ M. Donega,¹⁹ P. Dong,⁸ J. Donini,⁴² T. Dorigo,⁴² S. Dube,⁵¹ K. Ebina,⁵⁶
 J. Efron,³⁸ J. Ehlers,¹⁹ R. Erbacher,⁷ D. Errede,²³ S. Errede,²³ R. Eusebi,⁴⁸ H.C. Fang,²⁸ S. Farrington,²⁹
 I. Fedorko,⁴⁵ W.T. Fedorko,¹³ R.G. Feild,⁵⁹ M. Feindt,²⁵ J.P. Fernandez,⁴⁷ R. Field,¹⁷ G. Flanagan,³⁴
 L.R. Flores-Castillo,⁴⁶ A. Foland,²¹ S. Forrester,⁷ G.W. Foster,¹⁶ M. Franklin,²¹ J.C. Freeman,²⁸ Y. Fujii,²⁶
 I. Furic,¹³ A. Gajjar,²⁹ M. Gallinaro,⁴⁹ J. Galyardt,¹² J.E. Garcia,⁴⁵ M. Garcia Sciveres,²⁸ A.F. Garfinkel,⁴⁷
 C. Gay,⁵⁹ H. Gerberich,²³ E. Gerchtein,¹² D. Gerdes,³³ S. Giagu,⁵⁰ G.P. di Giovanni,⁴³ P. Giannetti,⁴⁵ A. Gibson,²⁸
 K. Gibson,¹² C. Ginsburg,¹⁶ N. Giokaris,¹⁴ K. Giolo,⁴⁷ M. Giordani,⁵³ M. Giunta,⁴⁵ G. Giurgiu,¹² V. Glagolev,¹⁴
 D. Glenzinski,¹⁶ M. Gold,³⁶ N. Goldschmidt,³³ J. Goldstein,⁴¹ G. Gomez,¹¹ G. Gomez-Ceballos,¹¹
 M. Goncharov,⁵² O. González,⁴⁷ I. Gorelov,³⁶ A.T. Goshaw,¹⁵ Y. Gotra,⁴⁶ K. Goulianos,⁴⁹ A. Gresele,⁴²
 M. Griffiths,²⁹ S. Grinstein,²¹ C. Grossi-Pilcher,¹³ U. Grundler,²³ J. Guimaraes da Costa,²¹ C. Haber,²⁸
 S.R. Hahn,¹⁶ K. Hahn,⁴⁴ E. Halkiadakis,⁴⁸ A. Hamilton,³² B.-Y. Han,⁴⁸ R. Handler,⁵⁸ F. Happacher,¹⁸ K. Hara,⁵⁴
 M. Hare,⁵⁵ S. Harper,⁴¹ R.F. Harr,⁵⁷ R.M. Harris,¹⁶ K. Hatakeyama,⁴⁹ J. Hauser,⁸ C. Hays,¹⁵ H. Hayward,²⁹
 A. Heijboer,⁴⁴ B. Heinemann,²⁹ J. Heinrich,⁴⁴ M. Hennecke,²⁵ M. Herndon,⁵⁸ J. Heuser,²⁵ D. Hidas,¹⁵ C.S. Hill,¹⁰
 D. Hirschbuehl,²⁵ A. Hocker,¹⁶ A. Holloway,²¹ S. Hou,¹ M. Houlden,²⁹ S.-C. Hsu,⁹ B.T. Huffman,⁴¹ R.E. Hughes,³⁸
 J. Huston,³⁴ K. Ikado,⁵⁶ J. Incandela,¹⁰ G. Introzzi,⁴⁵ M. Iori,⁵⁰ Y. Ishizawa,⁵⁴ A. Ivanov,⁷ B. Iyutin,³¹ E. James,¹⁶
 D. Jang,⁵¹ B. Jayatilaka,³³ D. Jeans,⁵⁰ H. Jensen,¹⁶ E.J. Jeon,²⁷ M. Jones,⁴⁷ K.K. Joo,²⁷ S.Y. Jun,¹² T.R. Junk,²³
 T. Kamon,⁵² J. Kang,³³ M. Karagoz-Unel,³⁷ P.E. Karchin,⁵⁷ Y. Kato,⁴⁰ Y. Kemp,²⁵ R. Kephart,¹⁶ U. Kerzel,²⁵
 V. Khotilovich,⁵² B. Kilminster,³⁸ D.H. Kim,²⁷ H.S. Kim,²⁷ J.E. Kim,²⁷ M.J. Kim,¹² M.S. Kim,²⁷ S.B. Kim,²⁷
 S.H. Kim,⁵⁴ Y.K. Kim,¹³ M. Kirby,¹⁵ L. Kirsch,⁶ S. Klimentko,¹⁷ M. Klute,³¹ B. Knuteson,³¹ B.R. Ko,¹⁵
 H. Kobayashi,⁵⁴ K. Kondo,⁵⁶ D.J. Kong,²⁷ J. Konigsberg,¹⁷ K. Kordas,¹⁸ A. Korytov,¹⁷ A.V. Kotwal,¹⁵
 A. Kovalev,⁴⁴ J. Kraus,²³ I. Kravchenko,³¹ M. Kreps,²⁵ A. Kreymer,¹⁶ J. Kroll,⁴⁴ N. Krumnack,⁴ M. Kruse,¹⁵
 V. Krutelyov,⁵² S. E. Kuhlmann,² Y. Kusakabe,⁵⁶ S. Kwang,¹³ A.T. Laasanen,⁴⁷ S. Lai,³² S. Lami,⁴⁵ S. Lammel,¹⁶
 M. Lancaster,³⁰ R.L. Lander,⁷ K. Lannon,³⁸ A. Lath,⁵¹ G. Latino,⁴⁵ I. Lazzizzera,⁴² C. Lecci,²⁵ T. LeCompte,²
 J. Lee,⁴⁸ J. Lee,²⁷ S.W. Lee,⁵² R. Lefèvre,³ N. Leonardo,³¹ S. Leone,⁴⁵ S. Levy,¹³ J.D. Lewis,¹⁶ K. Li,⁵⁹
 C. Lin,⁵⁹ C.S. Lin,¹⁶ M. Lindgren,¹⁶ E. Lipeles,⁹ T.M. Liss,²³ A. Lister,¹⁹ D.O. Litvintsev,¹⁶ T. Liu,¹⁶ Y. Liu,¹⁹
 N.S. Lockyer,⁴⁴ A. Loginov,³⁵ M. Loreti,⁴² P. Loverre,⁵⁰ R.-S. Lu,¹ D. Lucchesi,⁴² P. Lujan,²⁸ P. Lukens,¹⁶
 G. Lungu,¹⁷ L. Lyons,⁴¹ J. Lys,²⁸ R. Lysak,¹ E. Lytken,⁴⁷ P. Mack,²⁵ D. MacQueen,³² R. Madrak,¹⁶ K. Maeshima,¹⁶
 P. Maksimovic,²⁴ G. Manca,²⁹ F. Margaroli,⁵ R. Marginean,¹⁶ C. Marino,²³ A. Martin,⁵⁹ M. Martin,²⁴ V. Martin,³⁷
 M. Martínez,³ T. Maruyama,⁵⁴ H. Matsunaga,⁵⁴ M.E. Mattson,⁵⁷ R. Mazini,³² P. Mazzanti,⁵ K.S. McFarland,⁴⁸
 D. McGivern,³⁰ P. McIntyre,⁵² P. McNamara,⁵¹ R. McNulty,²⁹ A. Mehta,²⁹ S. Menzemer,³¹ A. Menzione,⁴⁵

P. Merkel,⁴⁷ C. Mesropian,⁴⁹ A. Messina,⁵⁰ M. von der Mey,⁸ T. Miao,¹⁶ N. Miladinovic,⁶ J. Miles,³¹ R. Miller,³⁴ J.S. Miller,³³ C. Mills,¹⁰ M. Milnik,²⁵ R. Miquel,²⁸ S. Miscetti,¹⁸ G. Mitselmakher,¹⁷ A. Miyamoto,²⁶ N. Moggi,⁵ B. Mohr,⁸ R. Moore,¹⁶ M. Morello,⁴⁵ P. Movilla Fernandez,²⁸ J. Mülsenstädt,²⁸ A. Mukherjee,¹⁶ M. Mulhearn,³¹ Th. Muller,²⁵ R. Mumford,²⁴ P. Murat,¹⁶ J. Nachtman,¹⁶ S. Nahn,⁵⁹ I. Nakano,³⁹ A. Napier,⁵⁵ D. Naumov,³⁶ V. Necula,¹⁷ C. Neu,⁴⁴ M.S. Neubauer,⁹ J. Nielsen,²⁸ T. Nigmanov,⁴⁶ L. Nodulman,² O. Norniella,³ T. Ogawa,⁵⁶ S.H. Oh,¹⁵ Y.D. Oh,²⁷ T. Okusawa,⁴⁰ R. Oldeman,²⁹ R. Orava,²² K. Osterberg,²² C. Pagliarone,⁴⁵ E. Palencia,¹¹ R. Paoletti,⁴⁵ V. Papadimitriou,¹⁶ A. Papikonomou,²⁵ A.A. Paramonov,¹³ B. Parks,³⁸ S. Pashapour,³² J. Patrick,¹⁶ G. Pauleta,⁵³ M. Paulini,¹² C. Paus,³¹ D.E. Pellett,⁷ A. Penzo,⁵³ T.J. Phillips,¹⁵ G. Piacentino,⁴⁵ J. Piedra,⁴³ K. Pitts,²³ C. Plager,⁸ L. Pondrom,⁵⁸ G. Pope,⁴⁶ X. Portell,³ O. Poukhov,¹⁴ N. Pounder,⁴¹ F. Prakoshyn,¹⁴ A. Pronko,¹⁶ J. Proudfoot,² F. Ptchos,¹⁸ G. Punzi,⁴⁵ J. Pursley,²⁴ J. Rademacker,⁴¹ A. Rahaman,⁴⁶ A. Rakitin,³¹ S. Rappoccio,²¹ F. Ratnikov,⁵¹ B. Reisert,¹⁶ V. Rekovic,³⁶ N. van Remortel,²² P. Renton,⁴¹ M. Rescigno,⁵⁰ S. Richter,²⁵ F. Rimondi,⁵ K. Rinnert,²⁵ L. Ristori,⁴⁵ W.J. Robertson,¹⁵ A. Robson,²⁰ T. Rodrigo,¹¹ E. Rogers,²³ S. Rolli,⁵⁵ R. Roser,¹⁶ M. Rossi,⁵³ R. Rossin,¹⁷ C. Rott,⁴⁷ A. Ruiz,¹¹ J. Russ,¹² V. Rusu,¹³ D. Ryan,⁵⁵ H. Saarikko,²² S. Sabik,³² A. Safonov,⁷ W.K. Sakumoto,⁴⁸ G. Salamanna,⁵⁰ O. Salto,³ D. Saltzberg,⁸ C. Sanchez,³ L. Santi,⁵³ S. Sarkar,⁵⁰ K. Sato,⁵⁴ P. Savard,³² A. Savoy-Navarro,⁴³ T. Scheidle,²⁵ P. Schlabach,¹⁶ E.E. Schmidt,¹⁶ M.P. Schmidt,⁵⁹ M. Schmitt,³⁷ T. Schwarz,³³ L. Scodellaro,¹¹ A.L. Scott,¹⁰ A. Scribano,⁴⁵ F. Scuri,⁴⁵ A. Sedov,⁴⁷ S. Seidel,³⁶ Y. Seiya,⁴⁰ A. Semenov,¹⁴ F. Semeria,⁵ L. Sexton-Kennedy,¹⁶ I. Sfiligoi,¹⁸ M.D. Shapiro,²⁸ T. Shears,²⁹ P.F. Shepard,⁴⁶ D. Sherman,²¹ M. Shimojima,⁵⁴ M. Shochet,¹³ Y. Shon,⁵⁸ I. Shreyber,³⁵ A. Sidoti,⁴³ A. Sill,¹⁶ P. Sinervo,³² A. Sisakyan,¹⁴ J. Sjolin,⁴¹ A. Skiba,²⁵ A.J. Slaughter,¹⁶ K. Sliwa,⁵⁵ D. Smirnov,³⁶ J. R. Smith,⁷ F.D. Snider,¹⁶ R. Snihur,³² M. Soderberg,³³ A. Soha,⁷ S. Somalwar,⁵¹ V. Sorin,³⁴ J. Spalding,¹⁶ F. Spinella,⁴⁵ P. Squillacioti,⁴⁵ M. Stanitzki,⁵⁹ A. Staveris-Polykalas,⁴⁵ R. St. Denis,²⁰ B. Stelzer,⁸ O. Stelzer-Chilton,³² D. Stentz,³⁷ J. Strologas,³⁶ D. Stuart,¹⁰ J.S. Suh,²⁷ A. Sukhanov,¹⁷ K. Sumorok,³¹ H. Sun,⁵⁵ T. Suzuki,⁵⁴ A. Taffard,²³ R. Tafirout,³² R. Takashima,³⁹ Y. Takeuchi,⁵⁴ K. Takikawa,⁵⁴ M. Tanaka,² R. Tanaka,³⁹ M. Tecchio,³³ P.K. Teng,¹ K. Terashi,⁴⁹ S. Tether,³¹ J. Thom,¹⁶ A.S. Thompson,²⁰ E. Thomson,⁴⁴ P. Tipton,⁴⁸ V. Tiwari,¹² S. Tkaczyk,¹⁶ D. Toback,⁵² S. Tokar,¹⁴ K. Tollefson,³⁴ T. Tomura,⁵⁴ D. Tonelli,⁴⁵ M. Tönnesmann,³⁴ S. Torre,⁴⁵ D. Torretta,¹⁶ S. Tourneur,⁴³ W. Trischuk,³² R. Tsuchiya,⁵⁶ S. Tsuno,³⁹ N. Turini,⁴⁵ F. Ukegawa,⁵⁴ T. Unverhau,²⁰ S. Uozumi,⁵⁴ D. Usynin,⁴⁴ L. Vacavant,²⁸ A. Vaiciulis,⁴⁸ S. Vallecorsa,¹⁹ A. Varganov,³³ E. Vataga,³⁶ G. Velev,¹⁶ G. Veramendi,²³ V. Veszpremi,⁴⁷ T. Vickey,²³ R. Vidal,¹⁶ I. Vila,¹¹ R. Vilar,¹¹ I. Vollrath,³² I. Volobouev,²⁸ F. Würthwein,⁹ P. Wagner,⁵² R. G. Wagner,² R.L. Wagner,¹⁶ W. Wagner,²⁵ R. Wallny,⁸ T. Walter,²⁵ Z. Wan,⁵¹ M.J. Wang,¹ S.M. Wang,¹⁷ A. Warburton,³² B. Ward,²⁰ S. Waschke,²⁰ D. Waters,³⁰ T. Watts,⁵¹ M. Weber,²⁸ W.C. Wester III,¹⁶ B. Whitehouse,⁵⁵ D. Whiteson,⁴⁴ A.B. Wicklund,² E. Wicklund,¹⁶ H.H. Williams,⁴⁴ P. Wilson,¹⁶ B.L. Winer,³⁸ P. Wittich,⁴⁴ S. Wolbers,¹⁶ C. Wolfe,¹³ S. Worm,⁵¹ T. Wright,³³ X. Wu,¹⁹ S.M. Wynne,²⁹ A. Yagil,¹⁶ K. Yamamoto,⁴⁰ J. Yamaoka,⁵¹ Y. Yamashita,³⁹ C. Yang,⁵⁹ U.K. Yang,¹³ W.M. Yao,²⁸ G.P. Yeh,¹⁶ J. Yoh,¹⁶ K. Yorita,¹³ T. Yoshida,⁴⁰ I. Yu,²⁷ S.S. Yu,⁴⁴ J.C. Yun,¹⁶ L. Zanello,⁵⁰ A. Zanetti,⁵³ I. Zaw,²¹ F. Zetti,⁴⁵ X. Zhang,²³ J. Zhou,⁵¹ and S. Zucchelli⁵

(CDF Collaboration)

¹*Institute of Physics, Academia Sinica, Taipei, Taiwan 11529, Republic of China*

²*Argonne National Laboratory, Argonne, Illinois 60439*

³*Institut de Fisica d'Altes Energies, Universitat Autònoma de Barcelona, E-08193, Bellaterra (Barcelona), Spain*

⁴*Baylor University, Waco, Texas 76798*

⁵*Istituto Nazionale di Fisica Nucleare, University of Bologna, I-40127 Bologna, Italy*

⁶*Brandeis University, Waltham, Massachusetts 02254*

⁷*University of California, Davis, Davis, California 95616*

⁸*University of California, Los Angeles, Los Angeles, California 90024*

⁹*University of California, San Diego, La Jolla, California 92093*

¹⁰*University of California, Santa Barbara, Santa Barbara, California 93106*

¹¹*Instituto de Fisica de Cantabria, CSIC-University of Cantabria, 39005 Santander, Spain*

¹²*Carnegie Mellon University, Pittsburgh, PA 15213*

¹³*Enrico Fermi Institute, University of Chicago, Chicago, Illinois 60637*

¹⁴*Joint Institute for Nuclear Research, RU-141980 Dubna, Russia*

¹⁵*Duke University, Durham, North Carolina 27708*

¹⁶*Fermi National Accelerator Laboratory, Batavia, Illinois 60510*

¹⁷*University of Florida, Gainesville, Florida 32611*

¹⁸*Laboratori Nazionali di Frascati, Istituto Nazionale di Fisica Nucleare, I-00044 Frascati, Italy*

¹⁹*University of Geneva, CH-1211 Geneva 4, Switzerland*

- ²⁰Glasgow University, Glasgow G12 8QQ, United Kingdom
²¹Harvard University, Cambridge, Massachusetts 02138
²²Division of High Energy Physics, Department of Physics,
 University of Helsinki and Helsinki Institute of Physics, FIN-00014, Helsinki, Finland
²³University of Illinois, Urbana, Illinois 61801
²⁴The Johns Hopkins University, Baltimore, Maryland 21218
²⁵Institut für Experimentelle Kernphysik, Universität Karlsruhe, 76128 Karlsruhe, Germany
²⁶High Energy Accelerator Research Organization (KEK), Tsukuba, Ibaraki 305, Japan
²⁷Center for High Energy Physics: Kyungpook National University, Taegu 702-701; Seoul National University,
 Seoul 151-742; and SungKyunKwan University, Suwon 440-746; Korea
²⁸Ernest Orlando Lawrence Berkeley National Laboratory, Berkeley, California 94720
²⁹University of Liverpool, Liverpool L69 7ZE, United Kingdom
³⁰University College London, London WC1E 6BT, United Kingdom
³¹Massachusetts Institute of Technology, Cambridge, Massachusetts 02139
³²Institute of Particle Physics: McGill University, Montréal,
 Canada H3A 2T8; and University of Toronto, Toronto, Canada M5S 1A7
³³University of Michigan, Ann Arbor, Michigan 48109
³⁴Michigan State University, East Lansing, Michigan 48824
³⁵Institution for Theoretical and Experimental Physics, ITEP, Moscow 117259, Russia
³⁶University of New Mexico, Albuquerque, New Mexico 87131
³⁷Northwestern University, Evanston, Illinois 60208
³⁸The Ohio State University, Columbus, Ohio 43210
³⁹Okayama University, Okayama 700-8530, Japan
⁴⁰Osaka City University, Osaka 588, Japan
⁴¹University of Oxford, Oxford OX1 3RH, United Kingdom
⁴²University of Padova, Istituto Nazionale di Fisica Nucleare,
 Sezione di Padova-Trento, I-35131 Padova, Italy
⁴³LPNHE-Université de Paris 6/IN2P3-CNRS
⁴⁴University of Pennsylvania, Philadelphia, Pennsylvania 19104
⁴⁵Istituto Nazionale di Fisica Nucleare Pisa, Universities of Pisa,
 Siena and Scuola Normale Superiore, I-56127 Pisa, Italy
⁴⁶University of Pittsburgh, Pittsburgh, Pennsylvania 15260
⁴⁷Purdue University, West Lafayette, Indiana 47907
⁴⁸University of Rochester, Rochester, New York 14627
⁴⁹The Rockefeller University, New York, New York 10021
⁵⁰Istituto Nazionale di Fisica Nucleare, Sezione di Roma 1,
 University of Rome "La Sapienza," I-00185 Roma, Italy
⁵¹Rutgers University, Piscataway, New Jersey 08855
⁵²Texas A&M University, College Station, Texas 77843
⁵³Istituto Nazionale di Fisica Nucleare, University of Trieste/ Udine, Italy
⁵⁴University of Tsukuba, Tsukuba, Ibaraki 305, Japan
⁵⁵Tufts University, Medford, Massachusetts 02155
⁵⁶Waseda University, Tokyo 169, Japan
⁵⁷Wayne State University, Detroit, Michigan 48201
⁵⁸University of Wisconsin, Madison, Wisconsin 53706
⁵⁹Yale University, New Haven, Connecticut 06520

We report on a measurement of the inclusive jet production cross section in $p\bar{p}$ collisions at $\sqrt{s} = 1.96$ TeV using data collected with the upgraded Collider Detector at Fermilab in Run II (CDF II) corresponding to an integrated luminosity of 385 pb^{-1} . Jets are reconstructed using the k_T algorithm. The measurement is carried out for jets with rapidity $0.1 < |y^{\text{jet}}| < 0.7$ and transverse momentum in the range $54 < p_T^{\text{jet}} < 700 \text{ GeV}/c$. The measured cross section is in good agreement with next-to-leading order perturbative QCD predictions after the necessary non-perturbative parton-to-hadron corrections are included.

PACS numbers: PACS numbers 12.38.Aw, 13.85.-t, 13.87.-a

The measurement of inclusive jet production in $p\bar{p}$ collisions at $\sqrt{s} = 1.96$ TeV constitutes a test of perturbative QCD (pQCD) [1] predictions over more than eight orders of magnitude in cross section, and is sensitive to the presence of physics beyond the standard model [2].

The increased center-of-mass energy and integrated luminosity in Run II at the Tevatron make it possible to measure the cross section for jets with transverse momentum [3], p_T^{jet} , up to about 700 GeV/c , extending the p_T^{jet} range by more than 150 GeV/c compared with pre-

vious results [4]. This letter presents a new measurement of the inclusive jet production cross section as a function of p_T^{jet} for jets with $p_T^{\text{jet}} > 54 \text{ GeV}/c$ and rapidity [3] in the region $0.1 < |y^{\text{jet}}| < 0.7$, where jets are reconstructed with the k_T algorithm [5, 6]. Similar measurements have been carried out using cone-based jet algorithms in Run II [7]. However, the k_T algorithm has been widely used for precise QCD measurements at both e^+e^- and $e^\pm p$ colliders, and allows a well defined comparison to the theoretical predictions, without introducing additional parameters [6] in the calculations. The measurements are corrected for detector effects back to the particle (hadron) level [8] and compared to pQCD next-to-leading order (NLO) predictions [9]. A proper comparison with the theory requires corrections to account for non-perturbative contributions that become important at low p_T^{jet} . This could explain the marginal agreement observed in previous studies [10].

The CDF II detector is described in detail elsewhere [11]. Here, the sub-detectors most relevant for this analysis are briefly discussed. The detector has a charged particle tracking system immersed in a 1.4 T magnetic field, aligned coaxially with the beam line. A silicon microstrip detector provides tracking over the radial range 1.35 to 28 cm and covers the pseudorapidity [3] range $|\eta| \leq 2$. A cylindrical 3.1 m long open-cell drift chamber covers the radial range from 44 to 132 cm and provides full tracking coverage for $|\eta| \leq 1$. Segmented sampling calorimeters, arranged in a projective tower geometry, surround the tracking system and measure the energy flow of interacting particles in $|\eta| \leq 3.6$. The central barrel calorimeter [12, 13] covers the region $|\eta| < 1$. It consists of electromagnetic and hadronic calorimeters segmented into 480 towers of size 0.1 in η and 15° in ϕ . The measured energy resolution for electrons is $\frac{\sigma(E)}{E} = \frac{13.5\%}{\sqrt{E_T [\text{GeV}]}} \oplus 2\%$. The single-pion energy resolution, as determined from test-beam data, is $\frac{50\%}{\sqrt{E_T [\text{GeV}]}} \oplus 3\%$. A hadronic calorimeter complements the coverage of the central barrel calorimeter in the region $0.6 < |\eta| < 1.0$ and provides additional forward coverage out to $|\eta| < 1.3$. The forward region, $1.1 < |\eta| < 3.6$, is covered by scintillator-plate electromagnetic and hadronic calorimeters. Cherenkov counters in the region $3.7 < |\eta| < 4.7$ measure the number of inelastic $p\bar{p}$ collisions to compute the luminosity [14].

Monte Carlo event samples are used to determine the response of the detector and the correction factors to the hadron level. The generated samples are passed through a full CDF detector simulation (based on GEANT3 [15] where the GFLASH [16] package is used to simulate the energy deposition in the calorimeters) and then reconstructed and analyzed using the same analysis chain as for the data. Samples of simulated inclusive jet events have been generated using the PYTHIA 6.203 [17] and HERWIG 6.4 [18] Monte Carlo generators. CTEQ5L [19]

parton distribution functions (PDFs) are used for the proton and antiproton. The PYTHIA samples have been created using a special tuned set of parameters, denoted as PYTHIA-TUNE A, that includes enhanced contributions from initial-state gluon radiation and secondary parton interactions between proton/antiproton beam remnants. Tune A was developed with dedicated studies of the underlying event using the CDF Run I data [20], and describes the measured jet shapes in Run II [21].

The k_T algorithm is used to reconstruct jets from the energy depositions in the calorimeter towers with transverse momentum above $0.1 \text{ GeV}/c$. First, all towers are considered as protojets. The quantities $k_{T,i} = p_{T,i}^2$ and $k_{T,(i,j)} = \min(p_{T,i}^2, p_{T,j}^2) \cdot \Delta R_{i,j}^2 / D^2$, are computed for each protojet and pair of protojets respectively, where $p_{T,i}$ denotes the transverse momentum of the i^{th} protojet, $\Delta R_{i,j}$ is the distance ($y - \phi$ space) between each pair of protojets, and D is a parameter that approximately controls the size of the jet. All $k_{T,i}$ and $k_{T,(i,j)}$ values are then collected into a single sorted list. In this combined sorted list, if the smallest quantity is of the type $k_{T,i}$, the corresponding protojet is promoted to be a jet and removed from the list. Otherwise, if the smallest quantity is of the type $k_{T,(i,j)}$, the protojets are combined into a single protojet by summing up their four-vector components. The procedure is iterated over protojets until the list is empty. The jet transverse momentum, rapidity, and azimuthal angle are denoted as $p_{T,\text{CAL}}^{\text{jet}}$, $y_{\text{CAL}}^{\text{jet}}$, and $\phi_{\text{CAL}}^{\text{jet}}$, respectively. The same jet algorithm is applied to all the final-state particles in the Monte Carlo to search for jets at the hadron level. The resulting hadron-level jet variables are denoted as $p_{T,\text{HAD}}^{\text{jet}}$, $y_{\text{HAD}}^{\text{jet}}$, and $\phi_{\text{HAD}}^{\text{jet}}$.

The measurements presented in this letter correspond to a total integrated luminosity of $385 \pm 22 \text{ pb}^{-1}$. Events are selected online using three-level trigger paths [22] with different prescales. In the first-level trigger, a single trigger tower with E_T above 5 GeV or 10 GeV is required. In the second-level trigger, clusters are formed around the selected trigger towers, and a cluster with E_T above 15 to 90 GeV, depending on the trigger path, is required. In the third-level trigger, jets are reconstructed using a cone-based algorithm, and a jet with E_T above 20 to 100 GeV is required. Jets are then searched for using the k_T algorithm, as explained above, with $D = 0.7$. For each trigger data sample, the threshold on the minimum $p_{T,\text{CAL}}^{\text{jet}}$ is chosen in such a way that the trigger selection is fully efficient. The events are required to have at least one jet with rapidity in the region $0.1 < |y_{\text{CAL}}^{\text{jet}}| < 0.7$ and corrected transverse momentum (see below) above $54 \text{ GeV}/c$. The events are selected to have at least one reconstructed primary vertex with z -position within 60 cm around the nominal interaction point. In order to remove beam-related backgrounds and cosmics rays, the events are required to fulfill $\cancel{E}_T / \sqrt{\sum E_T} < F(p_{T,\text{CAL}}^{\text{leading jet}})$, where \cancel{E}_T denotes the missing transverse energy [23] and $\sum_i E_T^i$ is the total transverse energy of the event,

as measured using calorimeter towers with E_T^i above 100 MeV. The threshold function $F(p_{T,CAL}^{\text{leading jet}})$ is defined as $F(p_T^{\text{jet}}) = \min(2 + 0.0125 \times p_T^{\text{jet}}, 7)$, where $p_{T,CAL}^{\text{leading jet}}$ is the uncorrected transverse momentum of the leading jet (highest p_T^{jet}) and the units are GeV. This criterion is designed to preserve more than 95% of the QCD events, as determined from Monte Carlo studies. A visual scan for $p_{T,CAL}^{\text{jet}} > 400$ GeV/c showed no remaining backgrounds.

The measured jet transverse momentum includes additional contributions from multiple proton-antiproton interactions per bunch crossing at high instantaneous luminosity. The data were collected at instantaneous luminosities varying between $0.2 \times 10^{31} \text{ cm}^{-2} \text{s}^{-1}$ and $9.6 \times 10^{31} \text{ cm}^{-2} \text{s}^{-1}$. At the highest instantaneous luminosities, an average of two interactions per bunch crossing are produced. This mainly affects the measured cross section at low p_T^{jet} where the contributions are sizeable. In CDF, multiple interactions are identified via the presence of additional primary vertices reconstructed from charged particles. The measured jet transverse momenta are corrected for this effect by removing a certain amount of transverse momentum, ϵ , for each additional primary vertex. A value $\epsilon = 1.62^{+0.70}_{-0.46}$ GeV/c is determined from the data by requiring that, after the correction is applied, the ratio of cross sections at low and high instantaneous luminosities does not show any p_T^{jet} dependence.

The reconstruction of the jet variables in the calorimeter is studied using Monte Carlo. These studies indicate that the angular variables of a jet are reconstructed with no significant systematic shift and with a resolution better than 0.05 units in y and ϕ at low $p_{T,CAL}^{\text{jet}}$, improving as $p_{T,CAL}^{\text{jet}}$ increases. The measured jet transverse momentum systematically underestimates that of the hadron level jet, which is mainly attributed to the non-compensating nature of the calorimeter [24]. For jets with $p_{T,CAL}^{\text{jet}}$ about 50 GeV/c, the jet transverse momentum is reconstructed with an average shift of -19% and a resolution of 14%. The jet reconstruction improves as $p_{T,CAL}^{\text{jet}}$ increases. For jets with $p_{T,CAL}^{\text{jet}}$ about 500 GeV/c, the average shift is -5% and the resolution is about 7%. The bisector method [25] is employed to evaluate how well the Monte Carlo reproduces the measured jet energy resolutions. Data and Monte Carlo agree within a relative uncertainty of $\pm 8\%$ over the whole $p_{T,CAL}^{\text{jet}}$ range.

The measured $p_{T,CAL}^{\text{jet}}$ distribution is unfolded back to the hadron level using Monte Carlo event samples. PYTHIA-TUNE A provides a reasonable description of the different jet and underlying event quantities, and is used to determine the correction factors in the unfolding procedure. In order to avoid any bias on the correction factors due to the particular PDF set used, which translates into slightly different simulated $p_{T,CAL}^{\text{jet}}$ distributions, PYTHIA-TUNE A is re-weighted until it accurately follows the measured $p_{T,CAL}^{\text{jet}}$ spectrum. The unfolding is carried out in two steps. First, an average correction

is computed. The correlation $\langle p_{T,HAD}^{\text{jet}} - p_{T,CAL}^{\text{jet}} \rangle$ vs $\langle p_{T,CAL}^{\text{jet}} \rangle$ is used to extract correction factors which are then applied to the measured jets to obtain the corrected transverse momenta, $p_{T,COR}^{\text{jet}}$. A raw cross section is defined as $\frac{d^2\sigma}{dp_{T,COR}^{\text{jet}} dy_{CAL}^{\text{jet}}} = \frac{1}{\mathcal{L}} \frac{N_{\text{COR}}^{\text{jet}}}{\Delta p_{T,COR}^{\text{jet}} \Delta y_{CAL}^{\text{jet}}}$, where

$N_{\text{COR}}^{\text{jet}}$ denotes the number of jets in a given $p_{T,COR}^{\text{jet}}$ bin, $\Delta p_{T,COR}^{\text{jet}}$ is the size of the bin, $\Delta y_{CAL}^{\text{jet}}$ denotes the region in y_{CAL}^{jet} considered, and \mathcal{L} is the luminosity. Second, the measurements are corrected for acceptance and smearing effects using a bin-by-bin unfolding procedure, which also accounts for the efficiency of the selection criteria.

The unfolding factors, $U(p_{T,COR}^{\text{jet}}) = \frac{d^2\sigma/dp_{T,HAD}^{\text{jet}} dy_{HAD}^{\text{jet}}}{d^2\sigma/dp_{T,COR}^{\text{jet}} dy_{CAL}^{\text{jet}}}$, are extracted from Monte Carlo and applied to the measured $p_{T,COR}^{\text{jet}}$ distribution to obtain the final result. The factor $U(p_{T,COR}^{\text{jet}})$ increases with $p_{T,COR}^{\text{jet}}$ and varies between 1.04 at low $p_{T,COR}^{\text{jet}}$ and 1.3 at very high $p_{T,COR}^{\text{jet}}$.

A detailed study of the different systematic uncertainties was carried out [26]. The measured jet energies were varied by $\pm 2\%$ at low p_T^{jet} and $\pm 3\%$ at high p_T^{jet} to account for the uncertainty on the absolute energy scale in the calorimeter [27]. This introduces an uncertainty in the measured cross section which varies between $\pm 10\%$ at low p_T^{jet} and $^{+55\%}_{-40\%}$ at high p_T^{jet} . A $\pm 8\%$ uncertainty on the jet energy resolution introduces an uncertainty between $\pm 2\%$ at low p_T^{jet} and $\pm 8\%$ at high p_T^{jet} . The unfolding procedure was repeated using HERWIG instead of PYTHIA-TUNE A to account for the uncertainty on the modeling of the parton cascades and the jet fragmentation into hadrons. This translates into an uncertainty about $\pm 5\%$ at low p_T^{jet} . The unfolding procedure was also carried out using unweighted PYTHIA-TUNE A, to estimate the residual dependence on the p_T^{jet} spectrum. This introduces an uncertainty of $\pm 4\%$ above 400 GeV/c, which becomes negligible at lower p_T^{jet} . The quoted uncertainty on ϵ was taken into account. The effect on the measured cross section is less than $\pm 3\%$ and negligible for jets with p_T^{jet} above 200 GeV/c. An additional 5.8% uncertainty on the total luminosity is not included.

Figure 1 shows the measured cross section as a function of p_T^{jet} compared to NLO pQCD predictions. The data are reported in Table I. The cross section decreases by more than eight orders of magnitude as p_T^{jet} increases from 54 GeV/c up to about 700 GeV/c. The NLO pQCD predictions are computed using the JETRAD program [9] with CTEQ6.1M PDFs [28] and the renormalization and factorization scales (μ_R and μ_F) set to $\mu_0 = \max(p_T^{\text{jet}})/2$.

Different sources of uncertainty in the theoretical predictions were considered. The main contribution comes from the uncertainty on the PDFs and was computed using the Hessian method [29]. It varies from $^{+20\%}_{-10\%}$ at low p_T^{jet} , and $^{+7\%}_{-5\%}$ for p_T^{jet} about 100 GeV/c, to $^{+70\%}_{-30\%}$ at high p_T^{jet} , dominated by the limited knowledge of the

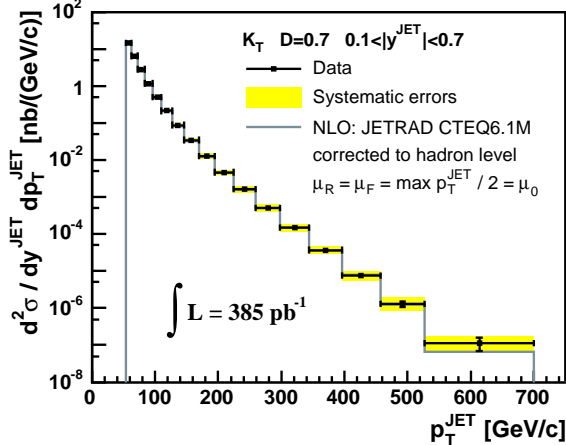


FIG. 1: Measured inclusive jet cross section (black dots) as a function of p_T^{jet} compared to NLO pQCD predictions (histogram). The shaded band shows the total systematic uncertainty on the measurement.

gluon PDF. An increase of μ_R and μ_F from μ_0 to $2\mu_0$ reduces the theoretical predictions by 2% at low p_T^{jet} and 8% at high p_T^{jet} . Values significantly smaller than μ_0 lead to unstable NLO results and were not considered.

The theoretical prediction includes a correction factor, $C_{\text{HAD}}(p_T^{\text{jet}})$, that approximately accounts for non-perturbative contributions from the underlying event and fragmentation into hadrons (see Table I). C_{HAD} was estimated, using PYTHIA-TUNE A, as the ratio between the nominal $p_{T,\text{HAD}}^{\text{jet}}$ distribution and the one obtained by turning off the interactions between proton and antiproton remnants and the fragmentation in the Monte Carlo. The parton-to-hadron correction shows a strong p_T^{jet} dependence and decreases as p_T^{jet} increases from about 1.2 at p_T^{jet} of 54 GeV/c, and 1.1 for p_T^{jet} about 100 GeV/c, to 1.02 at high p_T^{jet} . The uncertainty on C_{HAD} is about 13% at low p_T^{jet} and decreases up to 1.6% at high p_T^{jet} , as determined using HERWIG instead of PYTHIA-TUNE A.

Figure 2 shows the ratio data/theory as a function of p_T^{jet} . Good agreement is observed in the whole range in p_T^{jet} . A χ^2 test, where all the systematic uncertainties on the data are considered independent but fully correlated across different p_T^{jet} bins and the uncertainty on C_{HAD} is also included, gives a χ^2 probability of 56%. In addition, Figure 2 shows the ratio of pQCD predictions using MRST2004 [30] and CTEQ6.1M PDF sets, well inside the theoretical and experimental uncertainties.

In summary, we have presented results on inclusive jet production in $p\bar{p}$ collisions at $\sqrt{s} = 1.96$ TeV using the k_T algorithm, for jets with transverse momentum $p_T^{\text{jet}} > 54$ GeV/c and rapidity in the region $0.1 < |y^{\text{jet}}| < 0.7$, based on 385 pb^{-1} of CDF Run II data. The measured cross section is in agreement with NLO pQCD predictions after the necessary non-perturbative

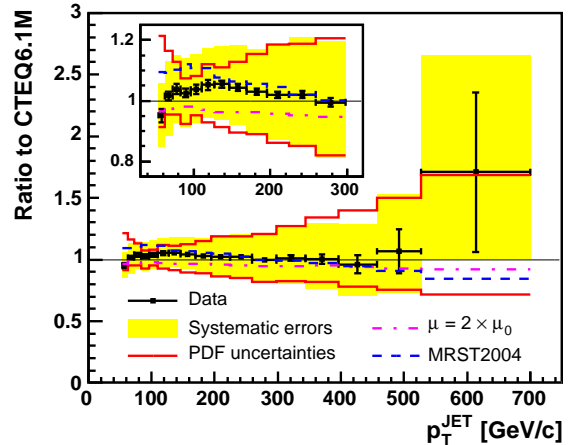


FIG. 2: Ratio Data/Theory as a function of p_T^{jet} . The enclosed figure expands the region $p_T^{\text{jet}} < 298$ GeV/c. The error bars (shaded band) show the total statistical (systematic) uncertainty on the data. A 5.8% uncertainty on the luminosity is not included. The solid lines indicate the PDF uncertainty on the theoretical prediction. The dashed line presents the ratio of MRST2004 and CTEQ6.1M predictions. The dotted-dashed line shows the ratio of predictions with $2\mu_0$ and μ_0 .

p_T^{jet} [GeV/c]	$\frac{d^2\sigma}{dp_T^{\text{jet}} dy^{\text{jet}}} \pm (\text{stat.}) \pm (\text{sys.})$	$C_{\text{HAD}} \pm (\text{stat.}) \pm (\text{sys.})$
	[nb/(GeV/c)]	parton \rightarrow hadron
54 - 62	$(14.6 \pm 0.2^{+1.6}_{-1.6}) \times 10^0$	$1.202 \pm 0.013 \pm 0.158$
62 - 72	$(6.53 \pm 0.04^{+0.75}_{-0.84}) \times 10^0$	$1.154 \pm 0.003 \pm 0.113$
72 - 83	$(2.81 \pm 0.02^{+0.30}_{-0.30}) \times 10^0$	$1.134 \pm 0.005 \pm 0.094$
83 - 96	$(1.18 \pm 0.01^{+0.13}_{-0.12}) \times 10^0$	$1.113 \pm 0.006 \pm 0.077$
96 - 110	$(5.04 \pm 0.04^{+0.56}_{-0.54}) \times 10^{-1}$	$1.098 \pm 0.004 \pm 0.066$
110 - 127	$(2.15 \pm 0.02^{+0.25}_{-0.22}) \times 10^{-1}$	$1.079 \pm 0.005 \pm 0.047$
127 - 146	$(8.81 \pm 0.05^{+1.04}_{-0.98}) \times 10^{-2}$	$1.064 \pm 0.003 \pm 0.037$
146 - 169	$(3.45 \pm 0.02^{+0.46}_{-0.41}) \times 10^{-2}$	$1.057 \pm 0.004 \pm 0.030$
169 - 195	$(1.28 \pm 0.01^{+0.17}_{-0.17}) \times 10^{-2}$	$1.047 \pm 0.003 \pm 0.023$
195 - 224	$(4.67 \pm 0.02^{+0.74}_{-0.68}) \times 10^{-3}$	$1.043 \pm 0.003 \pm 0.018$
224 - 259	$(1.63 \pm 0.01^{+0.30}_{-0.27}) \times 10^{-3}$	$1.039 \pm 0.004 \pm 0.015$
259 - 298	$(5.08 \pm 0.06^{+1.02}_{-0.93}) \times 10^{-4}$	$1.034 \pm 0.003 \pm 0.010$
298 - 344	$(1.50 \pm 0.03^{+0.36}_{-0.31}) \times 10^{-4}$	$1.030 \pm 0.005 \pm 0.008$
344 - 396	$(3.70 \pm 0.14^{+1.07}_{-0.89}) \times 10^{-5}$	$1.016 \pm 0.009 \pm 0.006$
396 - 457	$(7.50 \pm 0.55^{+2.52}_{-2.52}) \times 10^{-6}$	$1.017 \pm 0.018 \pm 0.009$
457 - 527	$(1.31 \pm 0.22^{+0.57}_{-0.42}) \times 10^{-6}$	$1.009 \pm 0.003 \pm 0.019$
527 - 700	$(1.14 \pm 0.43^{+0.63}_{-0.47}) \times 10^{-7}$	$1.018 \pm 0.002 \pm 0.016$

TABLE I: Measured inclusive jet differential cross section as a function of p_T^{jet} . An additional 5.8% uncertainty on the luminosity is not included. The parton-to-hadron correction factors, $C_{\text{HAD}}(p_T^{\text{jet}})$, are applied to the pQCD predictions.

parton-to-hadron corrections are taken into account.

We thank the Fermilab staff and the technical staffs of the participating institutions for their vital contributions. This work was supported by the U.S. Department of Energy and National Science Foundation; the Italian Istituto Nazionale di Fisica Nucleare; the Ministry of Education, Culture, Sports, Science and Technology of Japan;

the Natural Sciences and Engineering Research Council of Canada; the National Science Council of the Republic of China; the Swiss National Science Foundation; the A.P. Sloan Foundation; the Bundesministerium fuer Bildung und Forschung, Germany; the Korean Science and Engineering Foundation and the Korean Research Foundation; the Particle Physics and Astronomy Research Council and the Royal Society, UK; the Russian Foundation for Basic Research; the Comision Interministerial de Ciencia y Tecnologia, Spain; in part by the European Community's Human Potential Programme under contract HPRN-CT-2002-00292; and the Academy of Finland.

- [1] D.J. Gross and F. Wilczek, Phys. Rev. D **8**, 3633 (1973).
- [2] D. Stump *et al.*, JHEP **0310**, 046 (2003).
- [3] We use a cylindrical coordinate system about the beam axis in which θ is the polar angle and ϕ is the azimuthal angle. We define $E_T = E \sin\theta$, $p_T = p \sin\theta$, $\eta = -\ln(\tan(\frac{\theta}{2}))$, and $y = \frac{1}{2}\ln(\frac{E+p_z}{E-p_z})$.
- [4] T. Affolder *et al.* (CDF Collaboration), Phys. Rev. D **64**, 032001 (2001). [Erratum-*ibid.* D **65**, 039903 (2002)].
B. Abbott *et al.* (DØ Collaboration), Phys. Rev. Lett. **82**, 2451 (1999).
- [5] S. Catani *et al.*, Nucl. Phys. B **406**, 187 (1993).
- [6] S.D. Ellis and D.E. Soper, Phys. Rev. D **48**, 3160 (1993).
- [7] A. Abulencia *et al.* (CDF Collaboration), in preparation.
- [8] The hadron level in the Monte Carlo generators is defined using all final-state particles with lifetime above 10^{-11} s.

- [9] W.T. Giele, E.W.N. Glover and David A. Kosower, Nucl. Phys. B **403**, 633 (1993).
- [10] V.M. Abazov *et al.* (DØ Collaboration), Phys. Lett. B **525**, 211 (2002).
- [11] D. Acosta *et al.* (CDF Collaboration), Phys. Rev. D **71**, 032001 (2005).
- [12] L. Balka *et al.*, Nucl. Instrum. Meth. A **267**, 272 (1988).
- [13] S. Bertolucci *et al.*, Nucl. Instrum. Meth. A **267**, 301 (1988).
- [14] D. Acosta *et al.*, Nucl. Instrum. Meth., A **494**, 57 (2002).
- [15] R. Brun *et al.*, Tech. Rep. CERN-DD/EE/84-1, 1987.
- [16] G. Grindhammer, M. Rudowicz and S. Peters, Nucl. Instrum. Meth. A **290**, 469 (1990).
- [17] T. Sjöstrand *et al.*, Comp. Phys. Comm. **135**, 238 (2001).
- [18] G. Corcella *et al.*, JHEP **0101**, 010 (2001).
- [19] H.L. Lai *et al.*, Eur. Phys. J. C **12**, 375 (2000).
- [20] T. Affolder *et al.* (CDF Collaboration), Phys. Rev. D **65**, 092002 (2002).
- [21] D. Acosta *et al.* (CDF Collaboration), Phys. Rev. D **71**, 112002 (2005).
- [22] B. L. Winer, Int. J. Mod. Phys. A **16S1C**, 1169 (2001).
- [23] H_T is defined as the norm of $-\sum_i E_T^i \cdot \vec{n}_i$, where \vec{n}_i is the unit vector in the azimuthal plane that points from the beamline to the i-th calorimeter tower.
- [24] S.R. Hahn *et al.*, Nucl. Instrum. Meth. A **267**, 351 (1988).
- [25] P. Bagnaia *et al.* (UA2 Collaboration), Phys. Lett. B **144**, 283 (1984).
- [26] Olga Norniella, PhD. Thesis, University of Barcelona.
- [27] A. Bhatti *et al.*, hep-ex/0510047.
- [28] J. Pumplin *et al.*, JHEP **0207**, 012 (2002).
- [29] J. Pumplin *et al.*, Phys. Rev. D **65**, 014013 (2002).
- [30] A. D. Martin *et al.*, Eur. Phys. J. C **23**, 73 (2002).